

Nanosheets of Nonlayered Aluminum Metal–Organic Frameworks through a Surfactant-Assisted Method

Alexey Pustovarenko, Maarten G. Goesten, Sumit Sachdeva, Meixia Shan, Zakariae Amghouz, Youssef Belmabkhout, Alla Dikhtiarenko, Tania Rodenas, Damla Keskin, Ilja K. Voets, Bert M. Weckhuysen, Mohamed Eddaoudi, Louis C. P. M. de Smet, Ernst J. R. Sudhölter, Freek Kapteijn, Beatriz Seoane,* and Jorge Gascon*

During the last decade, the synthesis and application of metal–organic framework (MOF) nanosheets has received growing interest, showing unique performances for different technological applications. Despite the potential of this type of nanolamellar materials, the synthetic routes developed so far are restricted to MOFs possessing layered structures, limiting further development in this field. Here, a bottom-up surfactant-assisted synthetic approach is presented for the fabrication of nanosheets of various nonlayered MOFs, broadening the scope of MOF nanosheets application. Surfactant-assisted preorganization of the metallic precursor prior to MOF synthesis enables the manufacture of nonlayered Al-containing MOF lamellae. These MOF nanosheets are shown to exhibit a superior performance over other crystal morphologies for both chemical sensing and gas separation. As revealed by electron microscopy and diffraction, this superior performance arises from the shorter diffusion pathway in the MOF nanosheets, whose 1D channels are oriented along the shortest particle dimension.

The synthesis of 2D nanomaterials has arisen keen interest within the scientific and technological communities.^[1–3] This interest originates from their unique physicochemical properties, highly desirable for a wide range of applications.^[2–4] Examples of 2D nanomaterials that have been synthesized as single- and few-layer nanosheets are graphene and its group 14 analogs, transition-metal dichalcogenides, boron nitride, 2D layered oxides and hydroxides,^[2,3] and recently, metal–organic frameworks (MOFs).^[5] The last example is particularly exciting: MOFs are crystalline coordination compounds built-up from metal atoms or clusters linked together by the organic ligands.^[6] Their metal–organic make-up allows for rich pre and postsynthetic chemistry, which in some


A. Pustovarenko, Dr. A. Dikhtiarenko, Prof. J. Gascon
King Abdullah University of Science and Technology
KAUST Catalysis Center
Advanced Catalytic Materials
Thuwal 23955, Saudi Arabia
E-mail: jorge.gascon@kaust.edu.sa

A. Pustovarenko, Dr. S. Sachdeva, M. Shan, Prof. E. J. R. Sudhölter,
Prof. F. Kapteijn, Prof. J. Gascon
Department of Chemical Engineering
Delft University of Technology
Van der Maasweg 9, 2629 HZ Delft, The Netherlands

Dr. M. G. Goesten
Department of Chemistry and Chemical Biology
Baker Laboratory
Cornell University
259 East Ave, NY 14850, USA

Dr. Z. Amghouz
Servicios Científico Técnicos
Universidad de Oviedo
Oviedo 33006, Spain

Dr. Y. Belmabkhout, Prof. M. Eddaoudi
King Abdullah University of Science and Technology
Functional Materials Design
Advanced Membranes & Porous Materials Center
Thuwal 23955, Saudi Arabia

 The ORCID identification number(s) for the author(s) of this article can be found under <https://doi.org/10.1002/adma.201707234>.

Dr. T. Rodenas
Heterogene Reaktionen
Max-Planck-Institut für Chemische Energiekonversion
Stifstrasse 34-36, D-45470 Mülheim an der Ruhr, Germany

D. Keskin
Department of Biomedical Engineering
University of Groningen and University Medical Center Groningen
Antonius Deusinglaan 1, 9713 AV Groningen, The Netherlands

I. K. Voets
Department of Chemical Engineering and Chemistry
Eindhoven University of Technology
P. O. Box 513, 5600 MB Eindhoven, The Netherlands

Prof. B. M. Weckhuysen, Dr. B. Seoane
Inorganic Chemistry and Catalysis group
Debye Institute for Nanomaterials Science
Utrecht University
Universiteitsweg 99, 3584 CG Utrecht, The Netherlands
E-mail: b.seoanedelacuesta@uu.nl

Dr. L. C. P. M. de Smet
Laboratory of Organic Chemistry
Wageningen University
Stippeneng 4, 6708 WE Wageningen, The Netherlands

DOI: 10.1002/adma.201707234

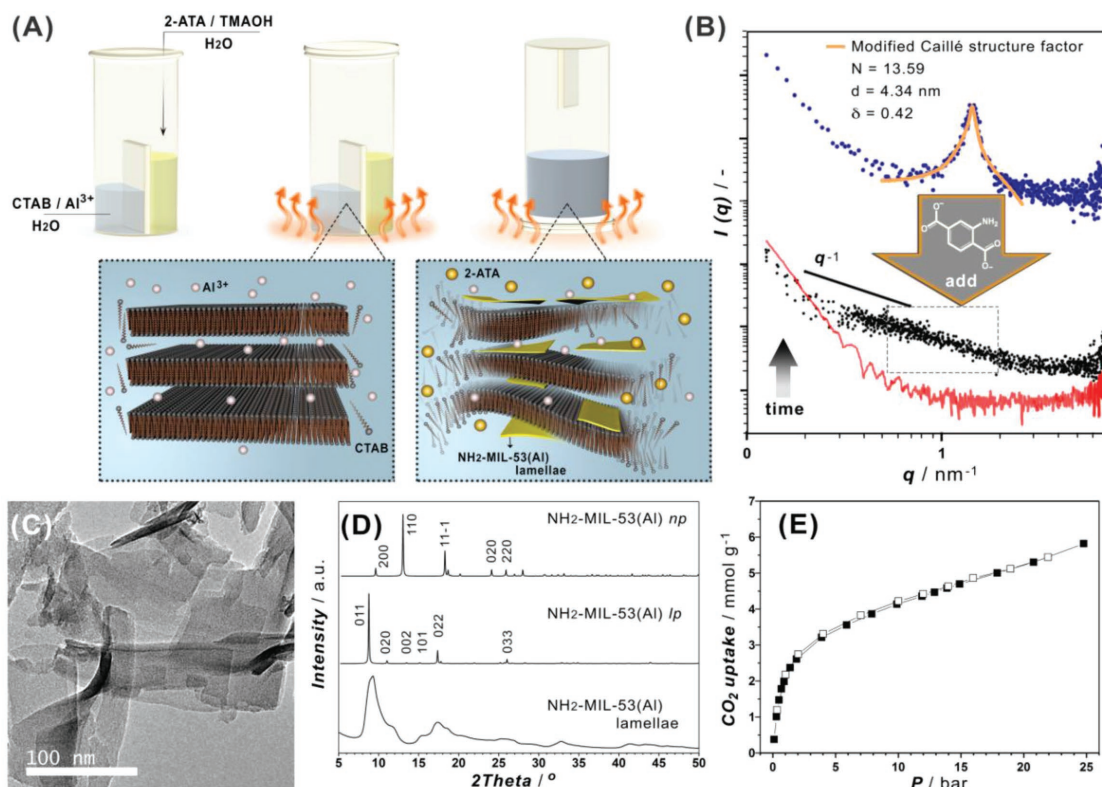


Figure 1. A) Schematic representation of the synthetic procedure developed and the formation mechanism of the $\text{NH}_2\text{-MIL-53(Al)}$ lamellae. The synthesis was performed from two different solutions: one containing the cationic surfactant hexadecyltrimethylammonium bromide (CTAB) and the metal precursor, the other the linker, 2-aminoterephthalic acid (2-ATA) and a base to deprotonate the linker, tetramethylammonium hydroxide (TMAOH). Both solutions were separately heated at 373 K, and mixed after 1 h. B) SAXS patterns acquired at 373 K for an aqueous solution of CTAB and $\text{Al}(\text{NO}_3)_3 \cdot 9\text{H}_2\text{O}$ before and after adding the deprotonated linker (blue and black points, respectively). The former pattern is fitted with the Modified Caillé structure factor, $N = 13.59$, $d = 4.34$ nm, $\delta = 0.42$. C) TEM image of the $\text{NH}_2\text{-MIL-53(Al)}$ lamellae. D) XRD pattern of the MOF nanosheets together with the simulated patterns for the np and lp configurations of $\text{NH}_2\text{-MIL-53(Al)}$. E) High-pressure CO_2 isotherm for $\text{NH}_2\text{-MIL-53(Al)}$ nanosheets at 273 K.

cases can lead to a degree of rational design.^[7] This opportunity for design, together with exceptional porosity, endows the MOFs with great potential in many different technological fields,^[8–13] their first commercial applications being recently announced.^[14]

MOF nanosheets have been prepared by various top-down and bottom-up approaches. As a top-down approach, the MOF nanosheets have been isolated by exfoliation,^[12,13,15,16] one of the most extended strategies to synthesize 2D nanomaterials.^[1–3] Bottom-up approaches rely on diffusion-mediated^[11] and templated synthesis^[2,8a,9,17,18–22] and the use of small capping agents or modulators to control crystal growth in certain directions.^[10,19,20] Despite the advances reported, the applicability of the synthetic methods developed so far is mainly restricted to the MOFs possessing a layered structure. These MOFs consist of stacked 2D layers, being more prone to the formation of nanosheets. However, this subfamily of compounds only embodies a small fraction of the MOF structures reported to date, severely limiting the potential of this promising type of 2D nanomaterials. To the best of our knowledge, only one very recent example has been reported so far on the top-down exfoliation of 3D MOFs.^[21] However, top-down approaches are often associated with particle fragmentation and reaggregation of the

detached sheets. A bottom-up approach for the synthesis of 3D MOF has never been reported.

Within this context, we report a novel bottom-up surfactant-assisted approach whereby several well-known nonlayered 3D Al-containing MOFs can be prepared as freestanding lamellae. Our approach is based on decoupling the surfactant-assisted preassembly of the metallic species in solution from the MOF synthesis, gaining control over the crystallization process. In particular, we have selected $\text{NH}_2\text{-MIL-53(Al)}$,^[22] CAU-10(Al) , and $\text{NH}_2\text{-CAU-10(Al)}$.^[23] Both MOF topologies, i.e., MIL-53 and CAU-10, are based on inorganic *trans*-connected $\text{AlO}_4(\mu_2\text{-OH})_2$ octahedra forming linear chains and *cis*-connected AlO_6 octahedra forming helical chains, respectively. For both topologies, these inorganic chains are connected through dicarboxylate linkers to make up the scaffold.^[23,24] In this work we demonstrate that the new 2D materials based on these MOF topologies provide a remarkable playground for membrane separation, chemical sensing, and device fabrication in general.

The bottom-up approach we developed here to synthesize $\text{NH}_2\text{-MIL-53(Al)}$ nanosheets makes use of surfactants to gain control over the MOF particle morphology.^[20] As schematically shown in **Figure 1a**, the synthesis was performed from two different solutions: i) one containing the cationic surfactant

hexadecyltrimethylammonium bromide (CTAB) and the metal precursor ($\text{Al}(\text{NO}_3)_3 \cdot 9\text{H}_2\text{O}$), ii) the other the deprotonated linker, 2-aminoterephthalic acid (2-ATA). Both the solutions were separately heated in order to reach the $\text{NH}_2\text{-MIL-53(Al)}$ synthesis temperature, 373 K, and mixed after 1 h. This allows for the surfactant-assisted preorganization of aluminum species, favored by the known ability of aluminum to form oligomeric structures in solution,^[25] prior to the MOF formation.

Small-angle X-ray Scattering (SAXS) provides some initial insight into the formation of the 2D material for $\text{NH}_2\text{-MIL-53(Al)}$. After being dissolved in a CTAB solution, the aluminum precursor, $\text{Al}(\text{NO}_3)_3 \cdot 9\text{H}_2\text{O}$, forms a preorganized vesicular system (blue points). The appearance of the quasi-Bragg peak, around $q = 1.6 \text{ nm}^{-1}$, is typical for an assembly of stacked sheets—a paracrystalline system.^[26] The line shape of the quasi Bragg peak, deviates from a Gaussian profile. It is broad, and sharpens toward the top. This indicates secondary disorder within the paracrystalline order; a root-mean-square deviation of the d -spacing, in this case the distance between the stacked sheets.^[27] We used a Caillé structure factor to approach this factor of disorder,^[28a] and obtained an accurate fitting of the quasi-Bragg peak (orange curve). The Caillé model takes into account bending fluctuations within the stacked-sheet system. Its central parameter, the Caillé parameter δ , is inversely proportional to the bulk modulus B and the bending modulus K of the sheets, $\delta \propto (KB)^{-1/2}$. The fitting produces a d -spacing of 4.34 nm and a Caillé parameter δ of 0.42. This signals an ordered yet soft system of the stacked sheets that engage in a process of bending deformations.^[28b] That this soft system is easily perturbed, is seen when linker, 2-ATA, is added. The system reorganizes, paracrystallinity breaks up and the scattering in the low- q region vanishes. Yet now, intensity falls off as $I(q) \propto q^{-1}$, which indicates that the scattering entities have retained the high aspect ratio we expect from the nanosheets with 1D channels. As confirmed by transmission electron microscopy (TEM), these entities indeed involve freestanding nanolamellae and display an extent of nanosheet bending and folding. We note that this was also reported for other cases of the MOF nanosheets.^[10,12,16,18] This effect of flexibility hinders an adequate determination of the particle size distribution, but it is clear that the nanosheets with submicron lateral dimensions are obtained. Furthermore, from atomic-force microscopy (Figure S2, Supporting Information) the lateral dimensions and thickness of the nanosheets can be assessed, being in the range 140–400 and 35–45 nm.

In order to optimize this synthetic methodology allowing the formation of $\text{NH}_2\text{-MIL-53(Al)}$ nanosheets, a systematic experimental study was performed by varying CTAB/ Al^{3+} ratios, ranging from 0.1 to 1.5 (Table S1 and Figure S3, Supporting Information). Among the different CTAB/ Al^{3+} ratios, we found 0.5 to be the optimal in the synthesis of MOF lamellae. This is demonstrated by TEM, X-ray diffraction (XRD), and gas adsorption (Figures S3 and S5, Supporting Information). XRD confirmed the formation of $\text{NH}_2\text{-MIL-53(Al)}$, the observed reflections corresponding to those expected for the large pore (lp) MOF configuration. This is noteworthy—since $\text{NH}_2\text{-MIL-53(Al)}$ is usually found in the narrow pore (np) form.^[29] Nevertheless, the relationship between crystal size and framework flexibility has been extensively studied revealing that with

changing the crystal size and surface in the flexible MOFs structures, the kinetic behavior of crystal structure transformation could be altered drastically.^[30] In particular, Kitagawa and co-workers demonstrated that crystal downsizing to the nanometre scale range can stabilize the transient pore configuration in the flexible MOF structures, leading to the further thermodynamic and/or kinetic suppression of lp–np phase transitions.^[30b] This behavior is not surprising and can be related to the fact that reducing crystal dimensions can generally accelerate guest diffusion/mobility and hence constrain the structural transformations of the flexible MOFs. Thus, we attribute the dominance of the lp configuration of $\text{NH}_2\text{-MIL-53(Al)}$ nanolamellae to both nanocrystal size and shorter diffusion length along the crystallographic a -direction.

CO_2 adsorption further corroborated this. The step in the CO_2 isotherm (Figure 1E), commonly attributed to the MIL-53 breathing behavior (starting at ≈ 7 bar for the submicron-sized $\text{NH}_2\text{-MIL-53(Al)}$ crystals),^[31] does not appear in the case of the MOF nanosheets. In fact, an isotherm archetypal for the rigid porous materials is obtained, the high uptake at low pressures corresponding to the filling of the MOF micropores. Furthermore, the slope observed at higher pressures can be attributed to the multilayer adsorption on the external surface area exposed by the MOF nanosheets. This interparticle porosity was also found for N_2 adsorption, where the H1-type hysteresis loops observed have been commonly encountered for other delaminated materials (Figure S5B, Supporting Information).^[11] Systematic study on the effect of low CTAB/ Al^{3+} ratio and the operating temperature is necessary to delineate the mechanism governing the dominance of the large pore configuration.

Once the suitability of our surfactant-assisted approach to synthesize the $\text{NH}_2\text{-MIL-53(Al)}$ nanosheets was confirmed, the question then arose, how the 1D diamond-shaped MIL-53 channels are oriented within the MOF lamellae. This orientation of the 1D channels has significant implications for different applications, as the diffusion pathway is much longer if the 1D channels run parallel to the surface of the nanosheets than if they do in the perpendicular direction. To gain some insight, high-resolution TEM (HRTEM) and selected-area electron diffraction (SAED) experiments were performed. Lattice fringes with interplanar distances of 13.4 and 16.2 Å were observed by HRTEM, corresponding to the (001) and (010) planes of $\text{NH}_2\text{-MIL-53(Al)}$, respectively (Figure 2). Moreover, SAED patterns were acquired along the [100] axis and showed diffraction spots corresponding to the ($0kl$) planes of the $\text{NH}_2\text{-MIL-53(Al)}$ nanosheets. Interestingly, comparison between the simulated and experimental SAED patterns and the $\text{NH}_2\text{-MIL-53(Al)}$ structure along [100] (Figure 2C and insets) points to an orientation of the 1D diamond-shaped channels perpendicular to the surface of the MOF nanosheets. Thus, besides the successful synthesis of the MOF nanosheets, a further advantage of this surfactant-assisted synthetic route is the orientation of the $\text{NH}_2\text{-MIL-53(Al)}$ channels along the shortest particle dimension. This interesting feature of $\text{NH}_2\text{-MIL-53(Al)}$ nanolamellae is presumably caused by preorganization of the CTAB/ Al^{3+} system. In order to understand the formation mechanism of the nanolamellae, dynamic light scattering (DLS) measurements were performed for CTAB/ Al^{3+} precursor mixtures. The corresponding data for DLS measurements are summarized

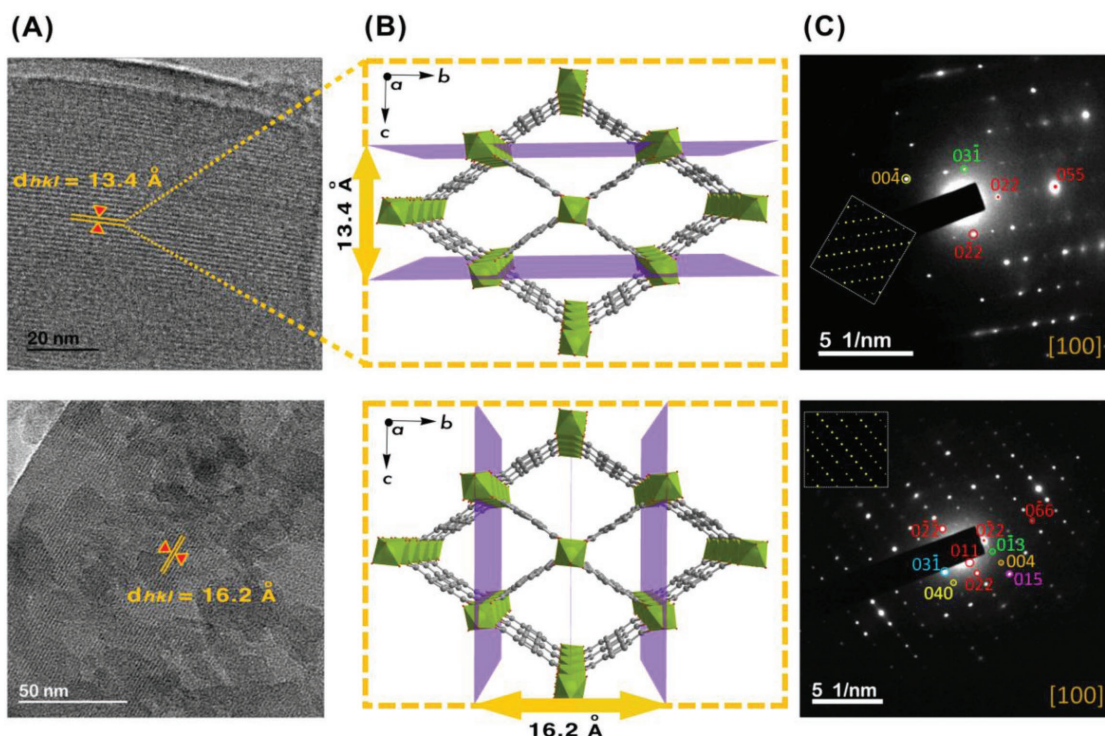


Figure 2. A) HRTEM images acquired for the NH₂-MIL-53(Al) nanosheets. Lattice fringes with interplanar distances of 13.4 and 16.2 Å were observed, corresponding to the crystallographic c - and b -axis, respectively. B) MIL-53 topology represented along the [100] direction. C) SAED patterns of NH₂-MIL-53(Al) lamellae showing the diffraction from $(0k)$ planes. Inset: simulated SAED pattern of NH₂-MIL-53(Al) along the [100] axis.

in the Supporting Information (Figure S1, Supporting Information). Notably, the value of critical micelle concentration observed by DLS technique ($8.2 \times 10^{-6} \text{ mol L}^{-1}$) is close to that determined by surface tension measurements. The increase in the hydrodynamic radius (R_h) above CMC suggests a progressive growth of CTAB micelles until reaching a maximum at $2.2 \times 10^{-2} \text{ mol L}^{-1}$ which corresponds to CTAB:Al³⁺ molar ratio of 0.1, first point of high CTAB concentration series (Figure S1D, Supporting Information). When compared to the measured thickness of independent lamellae, the hydrodynamic radii obtained from DLS are very similar. Thus, we hypothesize that at CTAB concentration $\approx 1.5 \times 10^{-4} \text{ mol L}^{-1}$, which corresponds to a CTAB/Al³⁺ ratio of 0.5, the aluminum oligomeric structures include themselves between the stacked CTAB lamellae micelles (Figure S1E, Supporting Information). As soon as the 2-aminoterephthalate anion is added to the system, the substitution of CTAB molecules in micelles by the linker occurs, initiating the formation of NH₂-MIL-53(Al) following the stacking predefined by the CTAB micelle (Figure S1F, Supporting Information) and resulting in pore alignment along the channel direction.

Exploring the versatility of this synthetic approach, this surfactant-assisted method was applied to two different well-known Al-containing MOFs, bearing different functionalities, namely CAU-10(Al) and NH₂-CAU-10(Al). Similarly to NH₂-MIL-53(Al) nanosheets (vide supra), screening of different CTAB/Al³⁺ ratios led to optimum values of 0.5 for CAU-10(Al) and 0.6 for NH₂-CAU-10(Al), suggesting that preorganization of Al is crucial for the successful synthesis of nanosheets. The XRD patterns of the product for this CTAB/Al³⁺ ratio demonstrated

formation of CAU-10(Al) and NH₂-CAU-10(Al) (Figure S6, Supporting Information), while SEM images evidenced the formation of MOF lamellae. In this case, however, the as-synthesized nanosheets were stacked into larger MOF particles with lateral dimensions of 2.5 ± 0.2 and $250 \pm 25 \text{ nm}$ for CAU-10(Al) and NH₂-CAU-10(Al), respectively (Figure S8, Supporting Information). Interestingly, mild sonication of these stacked particles in tetrahydrofuran (THF) for 40 min led to exfoliation. Indeed, the supernatant of the product obtained exhibits the Tyndall effect with laser beam irradiation, pointing to the high dispersion of particles of hundreds of nanometers in the colloidal suspension. Atomic force microscopy (AFM) confirmed that CAU-10(Al) nanosheets were isolated upon exfoliation (Figure 3D,E). It should be noted however that this occurs together with particle fragmentation, which leads to lamellae with reduced lateral dimensions.

Furthermore, next to the successful synthesis of several MOF topologies bearing different functionalities as nanosheets, preliminary data with other trivalent metals show that this approach could be extended to other MOFs, provided that the metal preassemblies in the presence of CTAB. Indeed, NH₂-MIL-53 containing different metals, i.e., Ga, have also shown the use of surfactants as a potential approach to gain control over the MOF particle morphology (Figure S11, Supporting Information). Collectively, these results underscore the potential of our surfactant-assisted method to synthesize lamellae of different nonlayered Al-containing MOFs. This complements the existing methods to synthesize MOF nanosheets, with a unique method for a bottom-up synthesis of MOF lamellae for topologies with a prevalent isotropic growth.

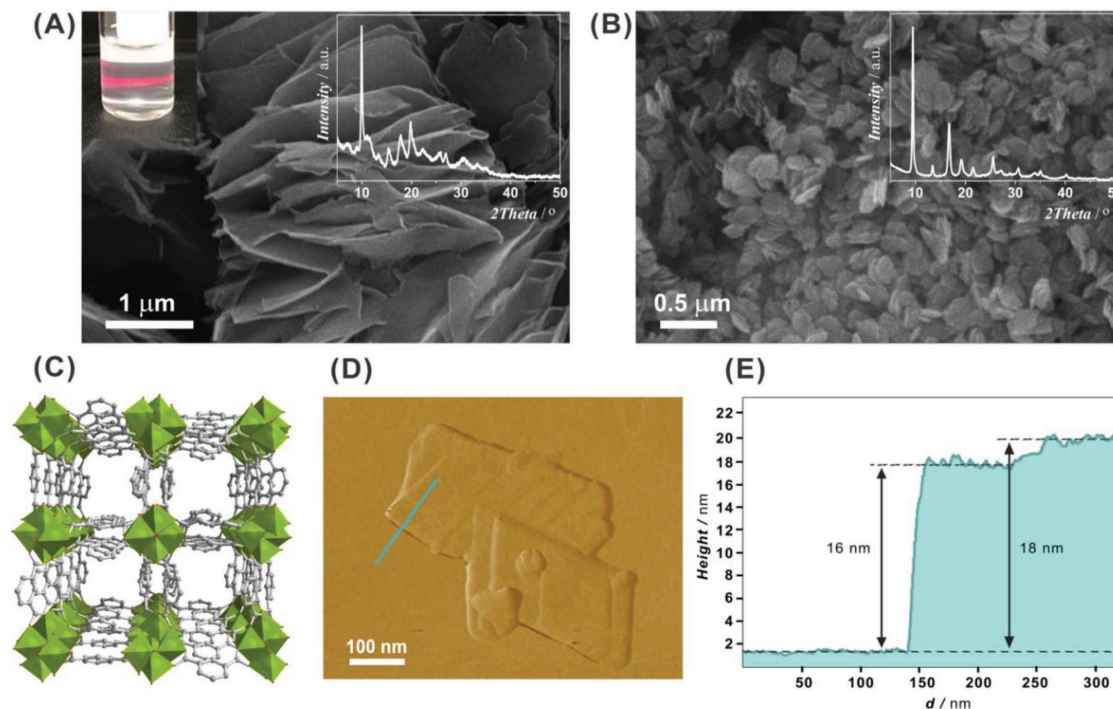


Figure 3. SEM images of the as-synthesized bulk particles of A) CAU-10(Al) and B) NH₂-CAU-10(Al) synthesized for a CTAB/Al³⁺ ratio of 0.5 and 0.6, respectively. Insets: Photograph demonstrating the Tyndall effect for the CAU-10(Al) nanosheets colloidal suspension obtained upon sonication and XRD patterns of A) CAU-10(Al) and B) NH₂-CAU-10(Al). C) Crystalline structure of CAU-10(Al) viewed along *c*-axis and showing the channel system. Aluminum, oxygen, and carbon atoms are shown in green, red, and gray, respectively. Hydrogen atoms have been omitted for clarity. D) AFM image of the exfoliated CAU-10(Al) nanosheets. E) Height profile corresponds to the blue line shown in the AFM image.

NH₂-MIL-53(Al) nanosheets and nanoparticles (Figure 1; Figure S12, Supporting Information) were applied to gas separation and molecular recognition applications to assess the potential of MOF lamellae as materials with superior performance. In the application of MOFs for gas separation, the use of MOFs as fillers in the MOF-based mixed-matrix membranes (MMMs), a blend of the MOF particles in a polymeric matrix, has shown great potential.^[32] Specifically, the use of MOF nanosheets as fillers has been recently identified by some of us

as a particular attractive strategy to synthesize advanced composite membranes for gas separation.^[11]

Matrimid-based MMMs containing NH₂-MIL-53(Al) with two different morphologies: nanoparticles and nanosheets were prepared. Figure 4A and Table S3 (Supporting Information) show the performance of these membranes in the separation of an equimolar mixture of CO₂ and CH₄ at 308 K and 3 bar of transmembrane pressure difference. For both nanoparticle and nanosheet fillers, the membrane permeability

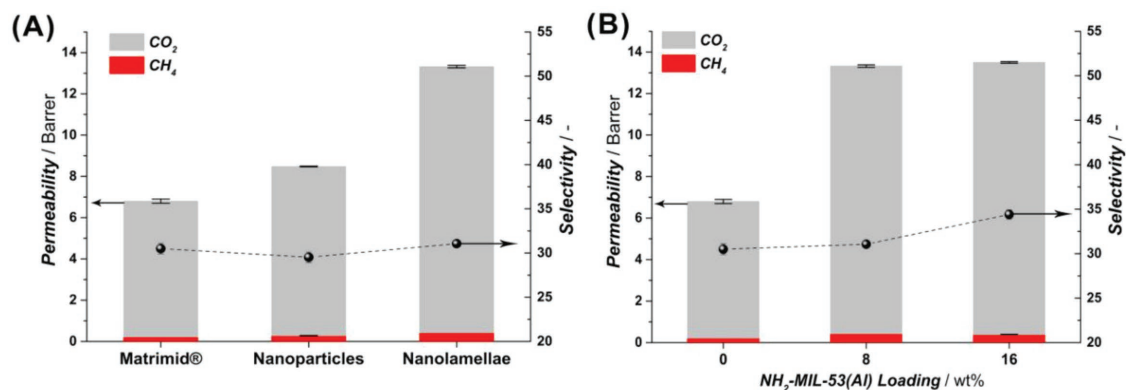


Figure 4. A) Influence of the filler morphology on the CO₂ and CH₄ permeability and on the CO₂/CH₄ selectivity for MMMs containing 8 wt% NH₂-MIL-53(Al) nanoparticles and lamellae at 308 K and a transmembrane pressure difference of 3 bar. B) Influence of the MOF loading on CO₂ and CH₄ permeability and CO₂/CH₄ mixed gas selectivity measured at 308 K and a transmembrane pressure difference of 3 bar for MMM containing NH₂-MIL-53 lamellae. Error bars correspond to standard deviation.

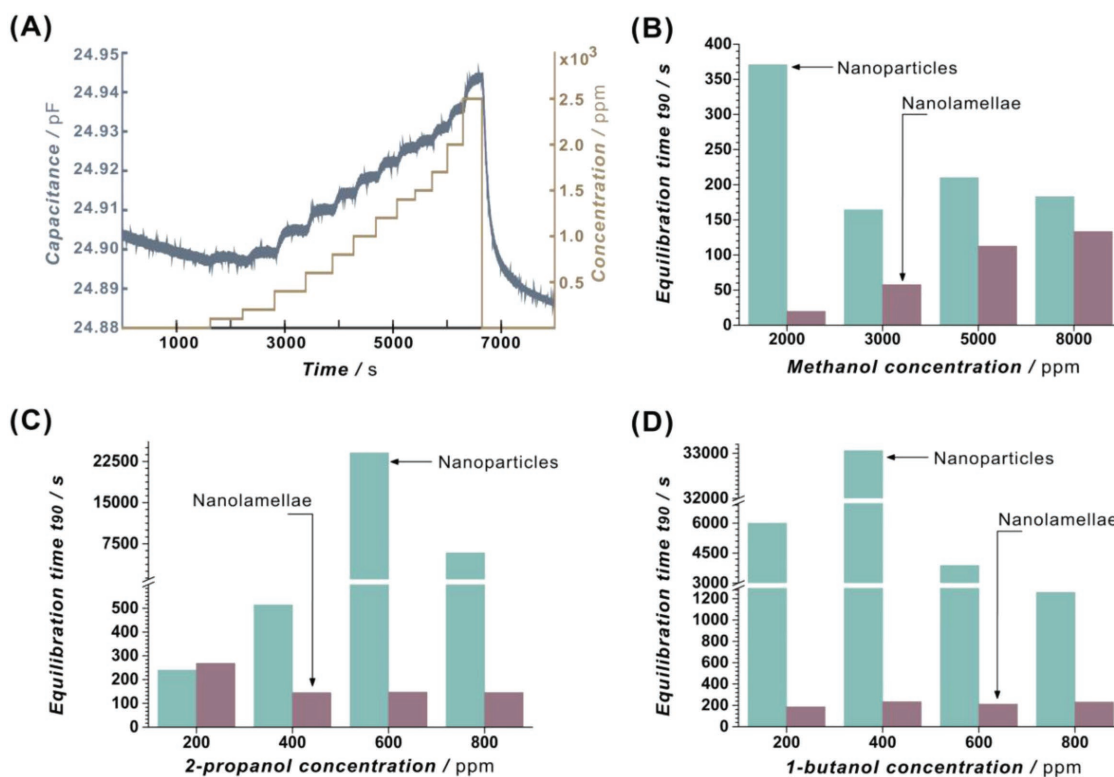


Figure 5. A) Capacitance sensing behavior of NH₂-MIL-53(Al) lamellae toward increasing concentration of 2-propanol. t_{90} equilibration time for NH₂-MIL-53(Al) lamellae and nanoparticles toward increasing concentration of: B) methanol, C) 2-propanol, and D) 1-butanol in a nitrogen flow.

increases upon 8 wt% MOF loading, which can be attributed to the additional gas transport pathways provided by the porous MOF. This increase in permeability is however more pronounced in the case of the NH₂-MIL-53(Al) nanosheets, reaching permeability values nearly twice than that for the bare polymer. The superior performance of the lamellae-based membranes can be ascribed to the more efficient utilization of the MOF's porosity. On the one hand, MOF nanosheets have been reported to orient parallel to the plane of the membrane, leading to a superior degree of coverage by the filler.^[11] On the other hand, the 1D channels of MIL-53 are oriented along the shortest particle dimension, perpendicular to this plane. This results in the orientation of the MOF channels along the direction of the gas flux, facilitating gas transport through the membrane. As for the selectivity, it remains unchanged upon MOF loading. This was expected given that NH₂-MIL-53(Al) is in its large pore form (vide supra), which is known to have moderate CO₂/CH₄ selectivity.^[33] Figure 4B further shows the influence of the NH₂-MIL-53(Al) nanosheets loading on the performance of the MMMs. Upon increasing the MOF loading, permeability remains unchanged while selectivity slightly increases. We hypothesize that this behavior is related to the rigidification of the polymeric chains surrounding the MOF nanosheets. This would result in higher selectivities and to a decrease in membrane permeability. Indeed, upon an increase in MOF loading from 8 to 16% the permeability remains unchanged, given that the rigidification of the polymeric chains counteracts the improved transport at higher MOF loading.

NH₂-MIL-53(Al) nanosheets were further investigated for its gas sensing properties toward alcohols. These materials were first drop-casted over meander-patterned, planar transducer devices (Figure S14, Supporting Information) to form a uniform layer over the sensing area (see the Experimental Section for details).^[34] The thickness of the layer was kept at 10 μ m to ensure that the majority of the electric field lines remain within the MOF layer, avoiding the influence of possible MOF coating variations on the sensor response. The coated devices were then exposed to different concentrations of alcohols (0–2500 ppm of methanol, 2-propanol, and 1-butanol) and the capacitive response was measured by impedance spectroscopy in a 4-probe configuration at 301 K. Figure 5 and Figure S15 (Supporting Information) clearly show a change in the sensing device capacitance upon alcohol exposure, the capacitance response increasing with higher alcohol concentrations. The response showed complete reversibility and a return to baseline in \approx 15 min over replacing the alcohol vapors in gas phase with dry N₂. Hence, the completely reversible and sensitive response of NH₂-MIL-53(Al) nanosheets-coated transducer devices toward methanol, 2-propanol, and 1-butanol indicated capabilities of these materials for sensing applications. Comparison of the sensor response with that of NH₂-MIL-53(Al) nanoparticle-coated devices learnt that the time required to reach half of the equilibration (t_{50}) and 90% of the equilibrium response (t_{90}) upon exposure to different alcohol concentrations was significantly reduced for the devices coated with the nanosheets. In the particular case of 2-propanol for instance, after exposure to 600 ppm, the response time was reduced by \approx 180 times

(Figure 5). This decrease in the response time can be attributed to the shorter diffusion pathways in the case of the MOF nanosheets, for which the 1D diamond-shaped $\text{NH}_2\text{-MIL-53(Al)}$ channels are oriented along the smallest particle dimension.

Our results underline the significance of the development of synthetic routes for the fabrication of the MOF nanosheets to reveal the true potential of these promising materials. We envision that the surfactant-assisted approach presented in this work will lead to the development of different methods to fabricate lamellae of MOFs that do not possess an intrinsic layered structure. This is crucial for the efficient utilization of the MOF materials as demonstrated here for gas separation and molecular recognition.

Experimental Section

Synthesis of $\text{NH}_2\text{-MIL-53(Al)}$ MOF Nanosheets: Freestanding $\text{NH}_2\text{-MIL-53(Al)}$ nanosheets were synthesized from two different aqueous solutions: one containing 0.84 g $\text{Al}(\text{NO}_3)_3 \cdot 9\text{H}_2\text{O}$ (2.2 mmol, Sigma-Aldrich, <98%) and 0.40 g CTAB (1.1 mmol, Sigma-Aldrich, <98%) and the other containing 0.29 g 2-aminoterephthalic acid (1.6 mmol, Sigma-Aldrich, 99%) and 2 mL tetramethylammonium hydroxide (TMAOH, Sigma-Aldrich, 25 wt%) in 10 and 5 mL distilled water, respectively. Both mixtures were separately stirred until complete dissolution and transferred into two different wall-separated compartments of a Teflon-lined (45 mL of total volume) stainless steel autoclave. The autoclave was then placed in an oven and heated to 373 K, temperature at which it was kept for 1 h. Then, the autoclave was turned upside down to let the two solutions from the separate chambers mix and react at 373 K for 16 h. After cooling, the formed yellow solid product was collected by centrifugation for 10 min at 6000 rpm and washed three times with water followed by another three times with ethanol through redispersion and centrifugation. The resulting washed material was finally transferred to a Petri dish and dried under vacuum at 353 K for 16 h or left suspended in THF (Sigma-Aldrich, anhydrous) until the preparation of the MOF composites.

Small-Angle X-Ray Scattering (SAXS): SAXS measurements were performed on a SAXSLAB GANESHA 300 XL SAXS system equipped with a GeniX 3D Cu Ultra Low Divergence micro focus sealed tube source producing X-rays with a wavelength $\lambda = 1.54 \text{ \AA}$ at a flux of $1 \times 10^8 \text{ ph s}^{-1}$ and a Pilatus 300K silicon pixel detector with 487×619 pixels of $172 \times 172 \text{ \mu m}$. Silver behenate was used for calibration of the beam centre and the q range. An aqueous solution containing $\text{Al}(\text{NO}_3)_3 \cdot 9\text{H}_2\text{O}$ and CTAB in 10 mL of distilled water (see solution described above) was loaded into a 1 mm borosilicate capillary (Hilgenberg GmbH, Germany). The solution was then heated up to 373 K, temperature at which small-angle (SAXS) patterns were acquired. Subsequently, a solution of deprotonated linker (see solution described above) was preheated at 373 K and added to the reaction mixture. Immediately after, another SAXS pattern was acquired.

Synthesis of MOF-Based Mixed-Matrix Membranes: MMMs were prepared following the procedure previously described by Rodenas et al.^[11] Briefly, 0.4 g of Matrimid 5218 (supplied by Huntsman Advanced Materials, $M_w \approx 80\,000 \text{ g mol}^{-1}$ and $M_n \approx 11\,000 \text{ g mol}^{-1}$) was added stepwise to a MOF suspension to obtain a final mass ratio solvent/(MOF+polymer) of 90/10, where the solvent selected was THF and the MOF $\text{NH}_2\text{-MIL-53(Al)}$. The $\text{NH}_2\text{-MIL-53(Al)}$ /Matrimid mass ratio was adjusted to achieve the desired MOF loading in the composite materials (i.e., 8 and 16 wt%). For the casting of membranes, the casting suspension was poured on a flat glass surface and shaped as a thin film with the help of a doctor Blade knife. The solvent was then removed by evaporation, first by natural convection at room temperature for 16 h and then under vacuum at 453 K for 24 h.

Gas Separation Experiments: Round-shaped membrane sheets with an area of 3.14 cm^2 were used to test the gas separation performance for two different gas mixtures. CO_2/CH_4 separation measurements

were performed for equimolar gas mixtures (50 mL min^{-1} of CO_2 and CH_4) at 308 K. He flow (3.3 mL min^{-1}) was used as sweep gas to increase the driving force over the membrane. The transmembrane pressure difference was adjusted in the range of 3–9 bar using a back-pressure controller at the retentate side, being the permeate side at atmospheric pressure. In all cases, separation selectivity and gas permeability values are reported after steady operation regime was reached.

Fabrication of MOF-Coated Devices: The sensor devices were fabricated over p-doped silicon substrates to obtain planar capacitive electrodes as described in our previous study.^[34b] Briefly, the devices were designed to obtain four parallel meander-patterned aluminum electrodes by photolithography with width of 0.52 \mu m and a gap of 1 \mu m . The total electrode area was obtained as $\approx 2.1 \text{ mm}^2$ leading to a high bare capacitance of the sensor devices ($\approx 22 \text{ pF}$). In order to prepare $\approx 10 \text{ \mu m}$ thick layers of $\text{NH}_2\text{-MIL-53(Al)}$ nanoparticles and nanosheets over these devices, 22.5 mg of MOF particles were dispersed in 480 mg THF. 5 \mu L of the prepared dispersions was drop-casted over the electrode area of the devices followed by drying in vacuum at 393 K.

Gas Sensing Studies: Sensing measurements were performed in a custom-built gas mixing and sensing equipment.^[34a] The addition of gas vapors to the measurement chamber was carried out by first generating a saturated stream of the vapors in dry N_2 gas and then further diluting it with N_2 to the desired concentration. The saturated stream was generated by passing the dry N_2 through a series of bubblers containing either methanol, 2-propanol or 1-butanol at room temperature. Changes in the concentration of the vapors in gas phase were analyzed by correlation with the changes in the capacitive response of the MOF-coated sensor devices. These measurements were performed by impedance spectroscopy using HP 4284A LCR Meter at a frequency of 20 kHz and voltage of 1 V in a four-probe configuration. The total gas flow rate and temperature during the measurement were kept constant at 200 mL min^{-1} and 301 K.

Supporting Information

Supporting Information is available from the Wiley Online Library or from the author.

Acknowledgements

B.S. gratefully acknowledges the Netherlands National Science Foundation (NWO) for her personal VENI grant. J.G. gratefully acknowledges the ERC Grant Agreement no. 335746, CrystEng-MOF-MMM. The authors also thank Mr. Duco Bosma and Mr. Bart Boshuizen from TU Delft for technical and LABVIEW support and Dr. Dimitri Soccol and Prof. Dirk J. Gravesteijn for providing us with the transducer platforms. I.K.V. acknowledges the Netherlands Organisation for Scientific Research (NWO ECHO-STIP Grant 717.013.005, NWOVIDI Grant 723.014.006) and the Dutch Ministry of Education, Culture and Science (Gravity Program 024.001.035) for financial support.

Conflict of Interest

The authors declare no conflict of interest.

Keywords

chemical sensing, crystal design, gas separation, metal–organic framework nanolamellae, molecular recognition

Received: December 12, 2017

Revised: March 22, 2018

Published online: May 17, 2018

- [1] a) R. Mas-Balleste, C. Gomez-Navarro, J. Gomez-Herrero, F. Zamora, *Nanoscale* **2011**, 3, 20; b) S. Z. Butler, S. M. Hollen, L. Y. Cao, Y. Cui, J. A. Gupta, H. R. Gutierrez, T. F. Heinz, S. S. Hong, J. X. Huang, A. F. Ismach, E. Johnston-Halperin, M. Kuno, V. V. Plashnitsa, R. D. Robinson, R. S. Ruoff, S. Salahuddin, J. Shan, L. Shi, M. G. Spencer, M. Terrones, W. Windl, J. E. Goldberger, *ACS Nano* **2013**, 7, 2898.
- [2] A. Gupta, T. Sakthivel, S. Seal, *Prog. Mater. Sci.* **2015**, 73, 44.
- [3] G. R. Bhimanapati, Z. Lin, V. Meunier, Y. Jung, J. Cha, S. Das, D. Xiao, Y. Son, M. S. Strano, V. R. Cooper, L. B. Liang, S. G. Louie, E. Ringe, W. Zhou, S. S. Kim, R. R. Naik, B. G. Sumpter, H. Terrones, F. N. Xia, Y. L. Wang, J. Zhu, D. Akinwande, N. Alem, J. A. Schuller, R. E. Schaak, M. Terrones, J. A. Robinson, *ACS Nano* **2015**, 9, 11509.
- [4] G. P. Liu, W. Q. Jin, N. P. Xu, *Angew. Chem., Int. Ed.* **2016**, 55, 13384.
- [5] a) P. Amo-Ochoa, L. Welte, R. González-Prieto, P. J. Sanz Miguel, C. J. Gómez-García, E. Mateo-Martí, S. Delgado, J. Gómez-Herrero, F. Zamora, *Chem. Commun.* **2010**, 46, 3262; b) L. Peng, J. Zhang, J. Li, B. Han, Z. Xue, G. Yang, *Chem. Commun.* **2012**, 48, 8688.
- [6] a) H. Li, M. Eddaoudi, M. O'Keeffe, O. M. Yaghi, *Nature* **1999**, 402, 276; b) S. R. Batten, N. R. Champness, X. M. Chen, J. Garcia-Martinez, S. Kitagawa, L. Ohrstrom, M. O'Keeffe, M. P. Suh, J. Reedijk, *Pure Appl. Chem.* **2013**, 85, 1715.
- [7] a) M. Eddaoudi, J. Kim, N. Rosi, D. Vodak, J. Wachter, M. O'Keeffe, O. M. Yaghi, *Science* **2002**, 295, 469; b) K. K. Tanabe, S. M. Cohen, *Chem. Soc. Rev.* **2011**, 40, 498.
- [8] a) Z. C. Zhang, Y. F. Chen, S. He, J. C. Zhang, X. B. Xu, Y. Yang, F. Nosheen, F. Saleem, W. He, X. Wang, *Angew. Chem., Int. Ed.* **2014**, 53, 12517; b) Y. X. Wang, M. T. Zhao, J. F. Ping, B. Chen, X. H. Cao, Y. Huang, C. L. Tan, Q. L. Ma, S. X. Wu, Y. F. Yu, Q. P. Lu, J. Z. Chen, W. Zhao, Y. B. Ying, H. Zhang, *Adv. Mater.* **2016**, 28, 4149.
- [9] a) G. W. Zhan, H. C. Zeng, *Adv. Funct. Mater.* **2016**, 26, 3268; b) M. T. Zhao, Y. X. Wang, Q. L. Ma, Y. Huang, X. Zhang, J. F. Ping, Z. C. Zhang, Q. P. Lu, Y. F. Yu, H. Xu, Y. L. Zhao, H. Zhang, *Adv. Mater.* **2015**, 27, 7372.
- [10] L. Y. Cao, Z. K. Lin, F. Peng, W. W. Wang, R. Y. Huang, C. Wang, J. W. Yan, J. Liang, Z. M. Zhang, T. Zhang, L. S. Long, J. L. Sun, W. B. Lin, *Angew. Chem., Int. Ed.* **2016**, 55, 4962.
- [11] T. Rodenas, I. Luz, G. Prieto, B. Seoane, H. Miro, A. Corma, F. Kapteijn, F. X. L. I. Xamena, J. Gascon, *Nat. Mater.* **2015**, 14, 48.
- [12] Y. Peng, Y. S. Li, Y. J. Ban, H. Jin, W. M. Jiao, X. L. Liu, W. S. Yang, *Science* **2014**, 346, 1356.
- [13] H. Xu, J. K. Gao, X. F. Qian, J. P. Wang, H. J. He, Y. J. Cui, Y. Yang, Z. Y. Wang, G. D. Qian, *J. Mater. Chem. A* **2016**, 4, 10900.
- [14] T. Faust, O. Farha, B. Hernandez, *Nat. Chem.* **2016**, 8, 990.
- [15] a) C. Hermosa, B. R. Horrocks, J. I. Martinez, F. Liscio, J. Gomez-Herrero, F. Zamora, *Chem. Sci.* **2015**, 6, 2553; b) P. Z. Li, Y. Maeda, Q. Xu, *Chem. Commun.* **2011**, 47, 8436; c) P. J. Saines, J. C. Tan, H. H. M. Yeung, P. T. Barton, A. K. Cheetham, *Dalton Trans.* **2012**, 41, 8585; d) J. C. Tan, P. J. Saines, E. G. Bithell, A. K. Cheetham, *ACS Nano* **2012**, 6, 615; e) P. J. Beldon, S. Tominaka, P. Singh, T. S. Dasgupta, E. G. Bithell, A. K. Cheetham, *Chem. Commun.* **2014**, 50, 3955; f) A. Gallego, C. Hermosa, O. Castillo, I. Berlanga, C. J. Gomez-Garcia, E. Mateo-Marti, J. I. Martinez, F. Flores, C. Gomez-Navarro, J. Gomez-Herrero, S. Delgado, F. Zamora, *Adv. Mater.* **2013**, 25, 2141; g) T. Araki, A. Kondo, K. Maeda, *Chem. Commun.* **2013**, 49, 552.
- [16] A. Kondo, C. C. Tiew, F. Moriguchi, K. Maeda, *Dalton Trans.* **2013**, 42, 15267.
- [17] a) Y. P. Yuan, W. Wang, L. G. Qiu, F. M. Peng, X. Jiang, A. J. Xie, Y. H. Shen, X. Y. Tian, L. D. Zhang, *Mater. Chem. Phys.* **2011**, 131, 358; b) W. T. Shang, X. C. Kang, H. Ning, J. L. Zhang, X. G. Zhang, Z. H. Wu, G. Mo, X. Q. Xing, B. X. Han, *Langmuir* **2013**, 29, 13168.
- [18] S. C. Junggeburth, L. Diehl, S. Werner, V. Duppe, W. Sigle, B. V. Lotsch, *J. Am. Chem. Soc.* **2013**, 135, 6157.
- [19] M. H. Pham, G. T. Vuong, F. G. Fontaine, T. O. Do, *Cryst. Growth Des.* **2012**, 12, 3091.
- [20] B. Seoane, S. Castellanos, A. Dikhtiarrenko, F. Kapteijn, J. Gascon, *Coord. Chem. Rev.* **2016**, 307, 147.
- [21] M. J. Cliffe, E. Castillo-Martínez, Y. Wu, J. Lee, A. C. Forse, F. C. N. Firth, P. Z. Moghadam, D. Fairen-Jimenez, M. W. Gaultois, J. A. Hill, O. V. Magdysyuk, B. Slater, A. L. Goodwin, C. P. Grey, *J. Am. Chem. Soc.* **2017**, 139, 5397.
- [22] J. Gascon, U. Aktay, M. D. Hernandez-Alonso, G. P. M. van Klink, F. Kapteijn, *J. Catal.* **2009**, 261, 75.
- [23] H. Reinsch, M. A. van der Veen, B. Gil, B. Marszalek, T. Verbiest, D. de Vos, N. Stock, *Chem. Mater.* **2013**, 25, 17.
- [24] T. Ahnfeldt, D. Gunzelmann, T. Loiseau, D. Hirsemann, J. Senker, G. Ferey, N. Stock, *Inorg. Chem.* **2009**, 48, 3057.
- [25] a) S. P. Bi, C. Y. Wang, Q. Cao, C. H. Zhang, *Coord. Chem. Rev.* **2004**, 248, 441; b) M. Haouas, C. Volklinger, T. Loiseau, G. Ferey, F. Taulelle, *Chem. Mater.* **2012**, 24, 2462.
- [26] X. C. Zhu, M. G. Goesten, A. J. J. Koekkoek, B. Mezari, N. Kosinov, G. Filonenko, H. Friedrich, R. Rohling, B. M. Szyja, J. Gascon, F. Kapteijn, E. J. M. Hensen, *Chem. Sci.* **2016**, 7, 6506.
- [27] A. Guinier, *X-Ray Diffraction in Crystals, Imperfect Crystals, and Amorphous Bodies*, Dover Publications, Mineola, NY, USA **1994**.
- [28] a) R. T. Zhang, R. M. Suter, J. F. Nagle, *Phys. Rev. E* **1994**, 50, 5047; b) G. Brotons, M. Dubois, L. Belloni, I. Grillo, T. Narayanan, T. Zemb, *J. Chem. Phys.* **2005**, 123, 024704.
- [29] A. Boutin, S. Couck, F. X. Coudert, P. Serra-Crespo, J. Gascon, F. Kapteijn, A. H. Fuchs, J. F. M. Denayer, *Microporous Mesoporous Mater.* **2011**, 140, 108.
- [30] a) A. Sabetghadam, B. Seoane, D. Keskin, N. Duim, T. Rodenas, S. Shahid, S. Sorribas, C. Le Guillouzer, G. Clet, C. Tellez, M. Daturi, J. Coronas, F. Kapteijn, J. Gascon, *Adv. Funct. Mater.* **2016**, 26, 3154; b) Y. Sakata, S. Furukawa, M. Kondo, K. Hirai, N. Horike, Y. Takashima, H. Uehara, N. Louvain, M. Meilikhov, T. Tsuruoka, S. Isoda, W. Kosaka, O. Sakata, S. Kitagawa, *Science* **2013**, 339, 193; c) P. Serra-Crespo, E. Gobechiya, E. V. Ramos-Fernandez, J. Juan-Alcaniz, A. Martinez-Joaristi, E. Stavitski, C. E. A. Kirschhock, J. A. Martens, F. Kapteijn, J. Gascon, *Langmuir* **2012**, 28, 12916.
- [31] C. Serre, S. Bourrelly, A. Vimont, N. A. Ramsahye, G. Maurin, P. L. Llewellyn, M. Daturi, Y. Filinchuk, O. Leynaud, P. Barnes, G. Ferey, *Adv. Mater.* **2007**, 19, 2246.
- [32] B. Seoane, J. Coronas, I. Gascon, M. E. Benavides, O. Karvan, J. Caro, F. Kapteijn, J. Gascon, *Chem. Soc. Rev.* **2015**, 44, 2421.
- [33] S. Couck, J. F. M. Denayer, G. V. Baron, T. Remy, J. Gascon, F. Kapteijn, *J. Am. Chem. Soc.* **2009**, 131, 6326.
- [34] a) S. Sachdeva, S. J. H. Koper, A. Sabetghadam, D. Soccol, D. J. Gravesteijn, F. Kapteijn, E. J. R. Sudhölter, J. Gascon, L. C. P. M. de Smet, *ACS Appl. Mater. Interfaces* **2017**, 9, 24926; b) S. Sachdeva, D. Soccol, D. J. Gravesteijn, F. Kapteijn, E. J. R. Sudholter, J. Gascon, L. C. P. M. de Smet, *ACS Sens.* **2016**, 1, 1188.